Available online at www.sciencedirect.com
SCIENCE DIRECT®
Flow Measurement and Instrumentation 15 (2004) 29–35
Flow Measurement and Instrumentation
www.elsevier.com/locate/flowmeasinst

Detection of improper installation from the sensor signal of vortex flowmeters

A.G. Rossberg [a,*], P. Riegler [b], F. Buhl [c], J. Herwig [c], J. Timmer [a]

[a] *Center for Data Analysis and Modeling (FDM), University of Freiburg, Eckerstrasse 1, 79018 Freiburg, Germany*
[b] *University of Applied Sciences Braunschweig/Wolfenbüttel, Salzdahlumer Str. 46/48, 38302 Wolfenbüttel, Germany*
[c] *ABB Automation Products GmbH, Göttingen, Germany*

Received 10 March 2003; received in revised form 27 May 2003; accepted 18 June 2003

Abstract

Effects of inappropriate installation can bias the measurements of flowmeters. For vortex flowmeters, a method is proposed to detect inappropriate installation of the flowmeter from the oscillatory signal of the vortex sensor. The method is based on assuming the process of vortex generation to be a generic, noisy, nonlinear oscillation, describable by a noisy Stuart–Landau equation, with a corresponding sensor signal that also contains higher harmonic excitations. By making use of the scaling properties of the Navier–Stokes Equation, the method was designed to be robust with respect to uncertainties in the fluid properties. The diagnostic functionality is demonstrated on measurement data. In the experiments, installation effects that lead to more than 0.5% error in the output of the flowmeter could clearly be detected.

Keywords: Vortex flowmeters; Installation effects; Nonlinearity; Oscillations

1. Introduction

Vortex flowmeters are widely used in industrial flowmetering. Particular advantages of this technology are the low cost of maintenance for the devices, their robustness to extreme condition, their low pressure drop, and their comparatively high accuracy [1,2]. Vortex flowmeters rely on the phenomenon of the von-Kármán vortex street: Downstream behind a *vortex shedder* or *bluff body* a regular chain of vortices is generated. The frequency of vortex formation f is approximately a linear function in the flow velocity or, for pipe flow, the volume flow rate Q. By measuring the frequency, Q can be determined. The most common method to detect the vortices is by a sensor measuring "pressure", i.e. reactive surface forces at the pipe boundaries, on "paddles" inserted into the flow, or at the bluff body itself—for example, by the piezo-electric effect. Alternatively, ultrasound barriers can be used [3–5]. There have also been proposals for hot-wire anemometers [6], polarimetric [7], optical [8], and electrostatic [9] sensors.

It is well known, that "the calibrations of flowmeters are dependent to some extent on the geometry of the pipework and fittings both upstream and downstream" [10]. Deviations from the specifications given by the manufacturer can bias the measured flow rate [11,12]. Similar effects result from deposits at or erosion of the bluff body or the pipe. Sometimes it is possible to avoid this susceptibility of the flowmeter to installation effects by constructive modifications [13]. But generally, it is a more realistic goal to develop flowmeters which can at least alert the user by issuing an automatic warning message. This could be a simple warning light, or a message on the field bus, which could then also contain information regarding the severity of the fault and an error estimate, a concept known as self-validating sensor (SEVA) [14].

Various schemes to detect faulty conditions have been proposed. Some of these rely on special hardware [15,16]. But, in order not to loose the technical advantages of vortex flowmetering, a detection on the basis of

* Corresponding author. Tel.: +49-761-203-7707; fax: +49-761-203-7700.
E-mail address: axel@fdm.uni-freiburg.de (A.G. Rossberg).

0955-5986/$ - see front matter © 2003 Elsevier Ltd. All rights reserved.
doi:10.1016/S0955-5986(03)00042-6

the signal of the vortex sensor alone is being sought. The methods that have been proposed for this end have in common that some quantitative characterizations of the signal are computed and compared with the values for normal conditions. Deviations are then identified as faults. Some of the proposed characterizations are based on a spectral analysis of the signal [17,18]. Others rely on the statistical analysis of intermediate results of the signal processing for the flow rate [19–22].

The method proposed here is based on a generic signal model which takes the nonlinear nature of the vortex dynamics explicitly into account. We argue that the characterizations derived on the basis of this signal model make use of essentially all information available. But there is another point that has to be addressed. Even for the unperturbed flow with correctly mounted flowmeter, the sensor signal depends on the flow rate and on various fluid properties. It seems that, in order to be able to detect deviant conditions, characterizations of the signal for a large number or "normal" conditions have to be recorded at the flowmeter, and the correct one has to be selected at each instant. The feasibility of this approach is therefore not immediately clear.

Here we show that, by making use of the scaling properties of the Navier–Stokes Equation, appropriate characterizations of the signal can be constructed which depend only weakly on the fluid properties or the flow rate, and are sensitive to inappropriate installation. In Section 2, the theoretical background for selecting these characterizations is laid out. Based on these results, specific characterizations are defined in Section 3. These are applied to experimental data in Section 4. Section 5 summarizes the results.

2. Modeling the sensor signal

2.1. Basic theory

The pipe flow through the vortex flowmeter is described by the Navier–Stokes Equation for incompressible media

$$\dot{\mathbf{v}} + (\mathbf{v}\cdot\nabla)\mathbf{v} = -\rho^{-1}\nabla p + \nu\nabla^2\mathbf{v}, \tag{1}$$

with the mass density ρ, the kinematic viscosity ν, and a velocity field $\mathbf{v} = \mathbf{v}(\mathbf{r}, t)$ and pressure field $p = p(\mathbf{r}, t)$ depending on space $\mathbf{r}$ and time t. The Navier–Stokes Equation is supplemented with the incompressibility condition

$$\nabla\cdot\mathbf{v} = 0 \tag{2}$$

and appropriate boundary conditions. When using suitably rescaled variables (indicated by a caret $\hat{}$), the Navier–Stokes Equation can be written in the dimensionless form

$$\mathrm{d}\hat{\mathbf{v}}/\mathrm{d}\hat{t} + (\hat{\mathbf{v}}\cdot\hat{\nabla})\hat{\mathbf{v}} = -\hat{\nabla}\hat{p} + Re^{-1}\hat{\nabla}^2\hat{\mathbf{v}}, \tag{3}$$

where $Re := 4Q/(\pi d\nu)$ is the Reynolds number, Q is the flow rate, and d is the pipe diameter[1]. This rescaled form correctly reflects the fact that the magnitude of the viscous term $Re^{-1}\hat{\nabla}^2\hat{\mathbf{v}}$ generally decreases with increasing Re, while the other three terms balance each other.

It is now important to notice [23] that neither the phenomenon of vortex shedding nor the short-term dynamics of the resulting von-Kármán vortex street do essentially depend on viscous effects (vortex shedding has been observed even in Bose–Einstein condensates, inviscid "quantum fluids" [24,25]). At high Reynolds numbers, viscous effects enter merely as small corrections, roughly of the order Re^{-1}. Of course, due to turbulence, the effective viscosity is larger than ν, and the decay of viscous effects is not quite as fast as Re^{-1}. Thin, viscously dominated boundary layers do also remain. But the overall effect persists. The higher the Reynolds number, the better the bulk vortex dynamics at not too large distance from the bluff body are described by the inviscid ($\nu\to 0$) limit. On the other hand, for small Re, viscous effects suppress vortex shedding.

A straightforward analysis shows that in the limit $\nu\to 0$ solutions of (1) and (2) are, up to scaling, independent of Q, with velocities $\sim Q$ and times $\sim Q^{-1}$. (We assume the flowmeter's geometry to be fixed, hence the length scale is fixed.) This is why the proportionality of the frequency of vortex shedding f and the flow rate Q is satisfied so well that, in simple vortex flowmeters, $f \times K^{-1}$, with an appropriate "K-factor" K, is used as a direct measure of Q without corrections. In modern vortex flowmeters, corrections to the scaling law are taken into account, e.g., by using a Re-dependent K. Since the Re-dependence of K is weak, it is easily determined and stored in the flowmeter based on measurements of a few data points only. Below we will make use of this approximate scaling law also for other characterizations of the flow field.

2.2. The signal model

It is well known [26–31], that the signal $x(t)$ of a sensor mounted behind a vortex shedder in a laminar flow can be described by the Stuart–Landau Equation

$$\dot{A} = (\varepsilon + i\omega_0)A - (g_r + ig_i)|A|^2A, \tag{4}$$

where $A = A(t)$ is the complex amplitude of the signal, $x(t) = A(t) + (\beta_r + i\beta_i)A^2(t) + (\gamma_r + i\gamma_i)A^3(t)$ + c.c. + h.o.t. (c.c.≡complex conjugate, h.o.t.≡higher order terms), and $\varepsilon,\omega_0,g_r,g_i,\beta_r,\beta_i,\gamma_r,\gamma_i$ are real parameters to be chosen appropriately with $\omega_0, g_r > 0$. With a symmetric setup of flow, bluff body, and sensor $\beta_r = \beta_i = 0$.

[1] The diameter of the bluff body in typical flowmeters is within the same order of magnitude.

Under the conditions where vortex flowmeters are used, the inlet flow is usually not laminar ($Re \approx 10^4 - 10^5$). The effect of turbulence can be modeled by supplementing Eq. (4) with a noise term, i.e.

$$\dot{A} = (\varepsilon + i\omega_0)A - (g_r + ig_i)|A|^2 A + \zeta, \tag{5}$$

where

$$\langle \zeta(t)\zeta(t') \rangle = 0, \text{ and } \langle \zeta(t)\bar{\zeta}(t') \rangle = 4F\delta(t-t'), \tag{6}$$

with $\langle \cdot \rangle$ denoting the expectation value and the overbar complex conjugation.

In order to take also the small-scale turbulence near the sensor into account, the a.c. part of the signal must now be expressed as

$$x(t) = A(t) + (\beta_r + i\beta_i)A^2(t) + (\gamma_r + i\gamma_i)A^3(t) + \text{c.c.} + \text{h.o.t.} + [\text{noise}]. \tag{7}$$

In principle, bifurcation theory leads to these results by the mere fact that the onset of vortex formation is a supercritical (=forward, continuous) Hopf bifurcation (=transition to oscillation from a steady state), either with [32] or without noise [33]. However, in other systems that satisfy these conditions, the range of validity of the Stuart–Landau Equation is limited to a small range in control parameter space near the bifurcation point (i.e. the point corresponding to $\epsilon = 0$).

An analysis of experimental time series reveals that for von-Kármán vortices in vortex flowmeters, the range of validity of Eqs. (5) and (6) extends over the complete working range of the flowmeter, at least in a semi-quantitative sense. This can be understood by the results of Section 2.1. Three ranges for the Reynolds number have to be distinguished: (i) At low Reynolds numbers, vortex shedding is suppressed by viscous damping. (ii) In the cross-over region vortex shedding sets in. (iii) At higher Reynolds numbers, the large-scale flow pattern is independent of *Re* up to scaling. Apparently, the cross-over region (ii) is narrow, and the transition from (ii) to (iii) is still close enough to the bifurcation point such that Eqs. (5) and (6) hold. By the scaling behaviors of the solution, Eqs. (5) and (6) are than valid over the complete range (iii). Hence, those characterizations of the sensor signal will be particularly useful which are sensitive to changes in the parameters in Eqs. (5)–(7).

2.3. Dependence of the signal on fluid properties

Regarding the dependency of the sensor signal on the material parameters of the fluid in the pipe, two aspects have to be distinguished: (a) dependencies due to the particular sensor technology at given flow field and (b) dependencies due to the effect of the fluid properties on the flow field itself. As far as (a) is concerned, we shall here assume that only the amplitude of the sensor signal depends on fluid parameters, i.e. the sensor signal is independent of the fluid up to a constant factor. For example, for sensors sensitive to reactive forces exerted by the fluid on the solid boundary (e.g., a paddle reaching into the fluid), the signal is, at fixed flow rate, proportional to the mass density of the fluid. For ultrasonic sensors, the phase modulation of the recorded wave train, for example, is inversely proportional to the square of the velocity of sound in the fluid.

In order to understand the dependence (b) of the signal on fluid parameters through the flow field, the well known scaling laws for the Navier–Stokes Eq. (1) can be used. The flow field at fixed volume flow depends on the fluid only through the kinematic viscosity. If $\mathbf{v}(\mathbf{r}, t) = \mathbf{v}_0(\mathbf{r}, t)$ (and a corresponding $p(\mathbf{r}, t)$) is a solution of (1) and (2) with viscosity $\nu = \nu_0$, then $\mathbf{v}(\mathbf{r},t) = \mathbf{v}'_0(\mathbf{r},t) = s\mathbf{v}_0(\mathbf{r},st)$ is a solution of (1) and (2) at viscosity $\nu = s\nu_0$ for any positive s. Obviously, the flow rate Q for $\mathbf{v}'_0$ is s times larger than the flow rate for $\mathbf{v}_0$ and the solutions $\mathbf{v}_0$ and $\mathbf{v}'_0$ have the same Reynolds number. Corresponding relations hold also for the probability distribution of the random velocity field in turbulent flow. Now, assume that, for a given viscosity ν_0, the (random) flow field $\mathbf{v}_0(\mathbf{r}, t)$ is known for all flow rates Q. Then the flow field for viscosity $\nu'_0 = s\nu_0$ at flow rate Q' is $\mathbf{v}(\mathbf{r},t) = \mathbf{v}'_0(\mathbf{r},t) = s\mathbf{v}_0(\mathbf{r},st)$, where $\mathbf{v}_0(\mathbf{r}, t)$ is the flow field for viscosity ν_0 at flow rate $Q = s^{-1}Q'$. When the dependence of the flow field on the flow rate is known for one viscosity, it is known for all viscosities.

It is desirable to preserve this scaling behavior for the sensor signal $x(t)$. The scaling behavior is preserved if $x(t)$ depends on $\mathbf{v}(\mathbf{r}, t)$ in such a way that, when $\mathbf{v}(\mathbf{r}, t) = \mathbf{v}_0(\mathbf{r}, t)$ leads to the signal $x(t) = x_0(t)$, then $\mathbf{v}(\mathbf{r}, t) = s\mathbf{v}_0(\mathbf{r}, st)$ leads to $x(t) = f(s)x_0(st)$. The function $f(s)$ is typically a power of s. The precise form of $f(s)$ is not relevant here, since the overall amplitude of $x(t)$ depends on the properties of the particular fluid anyway. Both reactive-force and ultrasound flow sensing lead to signals which are linear functionals in the instantaneous flow field [i.e. they do not depend on time derivatives of $\mathbf{v}(\mathbf{r}, t)$], and the scaling law for the signal is satisfied with both technologies.

3. Characteristic quantities

The strategy to detect improper mounting of the flowmeter is to obtain several quantitative characterizations, *features*, of the sensor signal and to verify if these features are in the range expected for proper mounting. Ideally, these features depend as little as possible on the flow rate and the fluid properties, and are sensitive to the geometry of the flow. Features that give the same value for the two signals $x(t) = x_0(t)$ and $x(t) = ux_0(st)$ with any positive u and s are particularly well suited for this task: by the discussion in Section 2.3, such features depend, with proper mounting, only on the Reynolds

number. By the results of Section 2.1, the flow field, and thus the signal, vary, up to scaling, only little with the Reynolds number. Since the features are assumed to be invariant under scaling, it follows that their dependence on the Reynolds number is weak.

The higher the number of independent features that can be used to classify the flow, the more reliable is the diagnosis. In order to estimate the number of independent features that can be extracted from the signal, we make use of the model (5)–(7). It has the nine free parameters $\varepsilon,\omega_0,g_r,g_i,F,\beta_r,\beta_i,\gamma_r,\gamma_i$. Two degrees of freedom depend on fluid properties and should not be used as characterizations. Thus, as far as our model of the signal is good,[2] there are at most seven independent features.

As a first step in analyzing the signal, the angular oscillation frequency $\omega = 2\pi f$ is determined using standard methods. From ω the flow rate can be obtained. Moreover, the period $2\pi/\omega$ is used as a natural time scale, which can be used to make the features invariant with respect to scaling of time. For the model (5) one has, with not too strong noise, $\omega \approx \omega_0 - g_i\varepsilon/g_r$.

For the subsequent analysis, the fundamental mode of oscillation is extracted from the signal. This is achieved by convoluting the signal with the Morlet wavelet

$$\omega(t) = \frac{\Delta\omega}{\sqrt{2\pi}}\exp\left(i\omega t - \frac{1}{2}(\Delta\omega t)^2\right), \tag{8}$$

where the band width $\Delta\omega = 0.2\omega$ was chosen such as to optimize the sensitivity of the characterizations. The result of the convolution, $z(t) = w(t) * x(t)$ is an estimate for the complex signal amplitude $A(t)$ of Eq. (5). It can be interpreted as the analytic signal corresponding to $x(t)$ after band-pass filtering. The filtering also eliminates most of the measurement noise.

From $z(t)$ the instantaneous frequency [34]

$$\omega_i(t) = \mathrm{Im}\left\{\frac{\dot{z}(t)}{z(t)}\right\} \tag{9}$$

and the phase

$$\phi(t) = \int_0^t \omega_i(t')\mathrm{d}t' \tag{10}$$

are obtained. As a measure for the phase stability of the oscillation, the feature D given by

$$D: = \frac{\mathrm{var}[\phi(t + 2\pi n/\omega) - \phi(t)]}{n} \tag{11}$$

with $n = 10$ is used. As is easily verified, D satisfies the scaling invariance as required. Using the model (5)–(7), one obtains $D \approx 4\pi F(g_r + g_i^2/g_r)/\varepsilon\omega$ in the weak-noise limit [35]. The feature

$$S: = \frac{\langle|z(t)|^2\rangle - \langle|z(t)|\rangle^2}{\langle|z(t)|\rangle^2}, \tag{12}$$

is a measure for the strength of fluctuations in the signal amplitude. It is estimated as $S \approx Fg_r/4\varepsilon^2$.

A feature quantifying the nonlinear frequency shift is, for example, given by

$$R: = \frac{\langle|z(t)|^2\omega_i(t)\rangle - \langle|z(t)|^2\rangle\langle\omega_i(t)\rangle}{\langle|z(t)|^2\rangle\langle w_i(t)\rangle}. \tag{13}$$

Approximately, one has $R \approx -2Fg_i/\varepsilon\omega$.

Finally, amplitude and phase of higher harmonics can be used to characterize the signal. This leads to the features

$$B = B_r + iB_i: = \frac{\langle\bar{z}(t)^2x(t)\rangle}{\langle|z(t)|\rangle^3} \tag{14}$$

and

$$G = G_r + iG_i: = \frac{\langle\bar{z}(t)^3x(t)\rangle}{\langle|z(t)|\rangle^4}. \tag{15}$$

For model (5)–(7), $B \approx (\beta_r + i\beta_i)(\varepsilon/g_r)^{1/2}$ and $G \approx (\gamma_r + i\gamma_i)(\varepsilon/g_r)$. Obviously, S, R, B, and G do also satisfy the desired scaling invariance. Using the approximation formulas given above, it is readily verified that the seven features that have been introduced span, up to scaling of time and amplitude, the full parameter space of the model (5)–(7). Introduction of further features would therefore not lead to significantly better characterizations.

In order to compare the features proposed here to those that could be obtained by a spectral analysis of the signal, it should be observed [36] that the general shape of main spectral peak depends little on the model parameters in Eq. (5). Only the center frequency, the width, and the height of the peak depend on the parameters. Regarding the higher harmonics, their amplitudes can be determined, but not their relative phases. Thus, using the same signal model as above, a spectral characterization of the signal would have to be restricted to three instead of seven quantities: the ratio of spectral width to center frequency for the fundamental mode, and the amplitudes of second and third harmonic relative to the fundamental.

4. Experimental results

4.1. Experimental setup

Measurements were performed on a vortex flowmeter VORTEX VT4000 DN150-ANSI[3], with water at 20 °C

[2] In fact, a faithful description requires corrections to the model. But these effects are small, and their quantitative characterization would be difficult.

[3] Produced by ABB Automation Products, Germany.

streaming steadily out of a large tank. Apart from the irregularities imposed for the experimental purpose, the mounting conditions conformed to the specifications of the device. The flow rate was measured independently using an inductive flowmeter mounted upstream. The flow rate and the oscillatory signal of the vortex sensor (frequencies in the range 2–13 Hz) were recorded at a sampling rate of at least 1 kHz using a digital data recorder (Viper-TA, Gould). Data analysis was performed off-line using the MATLAB software package.

4.2. The reference experiment

In order to verify the prediction that the features introduced above do in fact depend only little on *Re*, and to obtain reference data for a test for inappropriate mounting, the dependence of the features *D*, *S*, and *G* on the flow rate was determined. The setup used was always symmetric, so $B \equiv 0$. The feature *R* turned out to be too sensitive to external perturbations such as acoustic noise. It is therefore not used for the analysis.

The features were measured using time series of 1 min duration at flow rates Q = 19–132 m^3/h (Re = 4.7–32.5 $\times 10^4$), with the expectation values $\langle\cdot\rangle$ estimated by temporal averages. Measurements were repeated 8–43 times at each flow rate, and the average values of the features and their covariance matrix were calculated. The functional dependence of the features and the covariance matrix on the flow rate Q was then estimated using polynomial interpolation of the data. Leave-one-out cross validation was used to guard against overfitting. Third, fourth, and second order polynomials were used to fit *D*, *S*, and *G*, respectively. The full covariance matrix was taken into account to optimize the fit. For the covariance matrix itself a linear fit was used. Fig. 1 shows the measured and fitted reference data. As expected, the dependence on Q, respectively Re, is weak, especially for high Q ($Q > 60$ m^3/h).

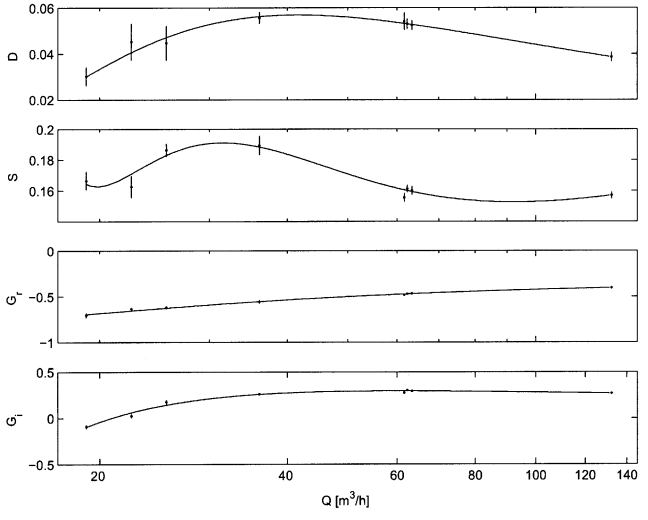

Fig. 1. The dependence of the features *D*, *S*, and $G = G_r + iG_i$, defined in Section 3 for a correctly mounted flowmeter. The points correspond to measurements ($1-\sigma$ errorbars), the curves to polynomial fits.

4.3. Detection of improper mounting

Data was collected with flowmeters mounted improperly in order to investigate if this could be detected from the measured features. For each setting, eight time series of 1 min duration were recorded at the flow rate Q = 50 m^3/h ($Re = 1.23 \times 10^5$). Two kinds of improper mounting were investigated: off-axis mounting of the flowmeter and a DIN/ANSI mismatch in the diameter of the flowmeter pipe (ANSI, d = 146.8 mm) and the upstream and downstream pipes (DIN, d = 159.3 mm). The features *D*, *S*, G_r turned out to be the most efficient for this purpose. Fig. 2 is as 3D scatter plot of the these features under all conditions. We evaluated this data under the assumption that, in practice, the kinematic viscosity or, equivalently, the Reynolds number, are not known. Instead, a maximum likelihood estimate of the Reynolds number is used, assuming correct mounting. As a result of the weak dependence of the features on the Reynolds number, the maximum likelihood estimates of *Re* have a rather low accuracy. Estimates of *Re* based on single 1-min time series have a standard errors of 40%. But, again due to the weak dependence, this accuracy is sufficient to obtain estimates of the expectation values of *D*, *S*, and G_r corresponding to some flow rate in Fig. 1 or, respectively, to some point on the curve in Fig. 2, that can be used to detect improper installation in the following way.

With respect to the estimates of the expectation values of the features and the corresponding covariance matrix $\mathbf{C}$, the deviations $\mathbf{e} := (\Delta D, \Delta S, \Delta G_r)^T$ of the measured features from their expectation values are calculated, and quantity χ^2 given by

$$\chi^2 = \mathbf{e}^T \mathbf{C}^{-1} \mathbf{e} \tag{16}$$

is obtained. This quantity is used as a criterion to distinguish appropriate from inappropriate mounting. Situations with χ^2 value larger than some threshold (which depends on the confidence level) are identified as inappropriate mounting. In practical, on-line applications, a moving average over χ^2 might be a more appropriate criterion.

The average χ^2 values for the data collected for each experimental setting are shown in Fig. 3. The value increases drastically as the mounting conditions worsen. For symmetry reasons, one expects the average χ^2 values to be an even function in the eccentricity for off-axis mounting. Hence, the effect of off-axis mounting sets in quadratically with the eccentricity and is initially weak. For all cases of off-axis mounting, the averages are significantly (α = 5%) increased compared to ordinary mounting. Only for the DIN/ANSI mismatch, the

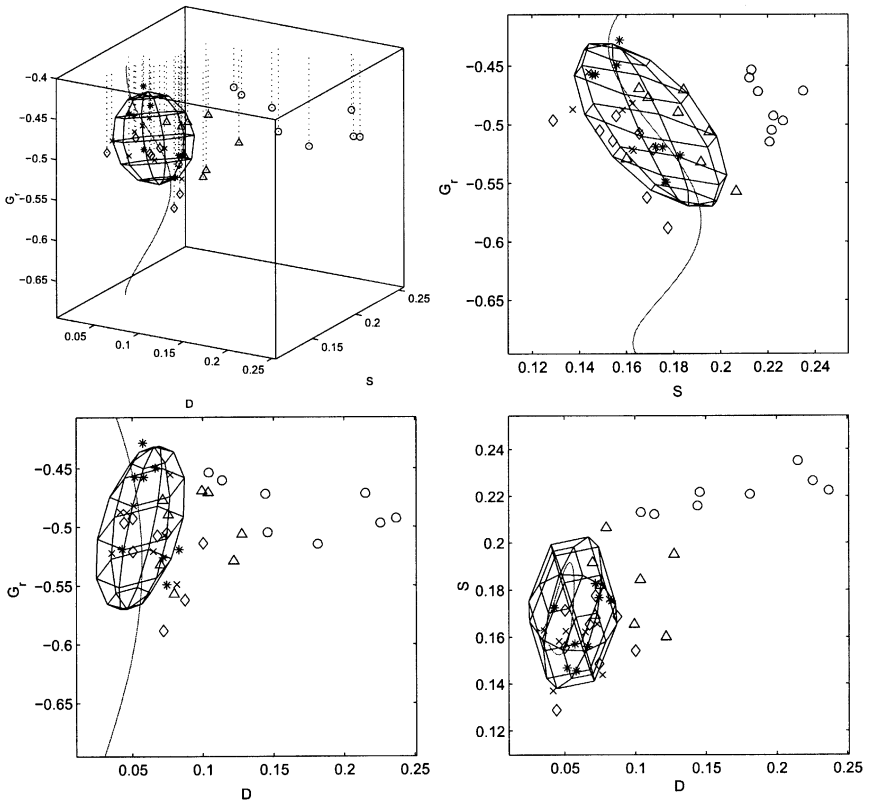

Fig. 2. A 3D view and 2D projections of the measured features D, S, and G_r for inappropriate mounting, see Section 4.3. In the 3D view data points are drawn as "hanging down" from the upper face of the enclosing box. Stars: correct mounting; ×: DIN/ANSI mismatch; diamonds, triangles, and circles: off-axis mounting with 5, 10, and 15 mm eccentricity. The solid curve corresponds to the expectation values for correct mounting, parameterized by the flow rate Q. The ellipsoid is the 95% confidence interval for correct mounting at $Q = 50$ m^3/h (assuming Gaussian errors).

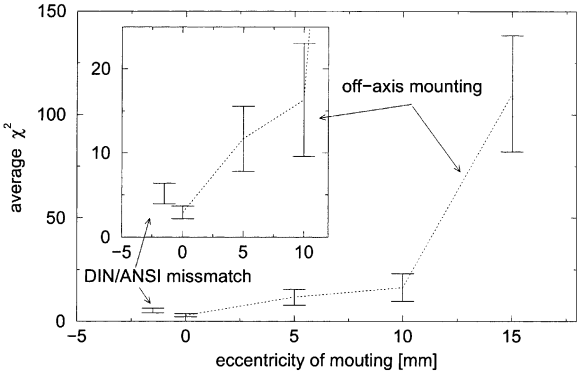

Fig. 3. Average values of χ^2 derived from the sensor signal in order to detect inappropriate mounting. The data point for DIN/ANSI mismatch was shifted to the left. The inset is a blowup of the low-χ^2 region.

hypotheses of an average χ^2 equal to the value for ordinary mounting could not be rejected ($p = 0.07$). A repetition of the experiment for $Q = 100$ m^3/h gave similar results.

In order to assess the sensitivity of the method, we note that the shift in the vortex frequency due to inappropriate mounting and, as a result, the error in the flowmeter reading, is larger than 0.5% only for the 10 and 15 mm eccentricity cases. These can clearly be identified by an increase in χ^2. Thus, as a conservative estimate, irregularities that lead to more than 0.5% error in the output of the flowmeter can be detected.

5. Conclusion

A method for detecting inappropriate installation of vortex flowmeters was demonstrated. The method is based on a general model of the sensor signal of the flowmeter. It is therefore expected to work also for other flowmeter geometries and to be able to detect several other kinds of faulty conditions, such as irregularities in the inlet or outlet piping, erosion of or depositions at the bluff body, or inhomogeneity of the fluid.

So far, the independence of the method from the fluid properties has not been verified experimentally. But the weak dependence of the scale-invariant features on the flow rate is a strong indication that the general theoretical considerations which lead to the predicted independence on the fluid material are correct.

Acknowledgements

We acknowledge generous support by the German Bundesministerium für Bildung und Forschung (BMBF), grants 13N7954, 13N7955.

References

[1] G.J. Blickley, Vortex flowmeters provide higher accuracy, low pressure drop, Contr. Eng. 42 (12) (1995) 59–64.
[2] E. Ribolini, Intelligent and mass flowmeters, InTech, USA 43 (2) (1996) 30.
[3] V. Hans, G. Poppen, E. von Lavante, S. Perpeet, Vortex shedding flowmeters and ultrasound detection: signal processing and influence of bluff body geometry, Flow Meas. Instrum. 9 (2) (1998) 79–82.
[4] T. Kawano, Y. Matsunaga, T. Andoh, A. Yasumatsu, Ultrasonic vortex flowmeter "ULTRA YEWFLOW-UYF200", Yokogawa Tech. Rep. 25, Yokogawa Electr. Comp., Japan, 1998.
[5] V. Hans, H. Windorfer, Comparison of pressure and ultrasound measurements in vortex flow meters, Measurement 33 (2) (2003) 121–133.
[6] D.V. Kratirov, S.M. Mekeshkin, N.I. Mikheev, V.M. Molochnikov, A.A. Ogarkov, Vortex-shedding flowmeter with improved characteristics in the region of low average-flow-rate velocity, Appl Energy: Russ. J. Fuel Power Heat Syst. 36 (3) (1998) 68–76 (Paralleledition of Energetika).
[7] M. Roszko, A.W. Domanski, M. Sierakowski, M. Swillo, Vortex flowmeter with polarimetric sensing, in: Proc. SPIE—Int. Soc. Opt. Eng., 3478, SPIE—Int. Soc. Opt. Eng, USA, 1998, pp. 457–462.
[8] S. Saito, M. Hashimoto, T. Wada, Development of Karman vortex flowmeter by use of laser diode, in: Proc. FLOMEKO 1993, 1993, pp. 335–340.
[9] A.K. El-Wahed, J.L. Sproston, The influence of shedder shape on the performance of the electrostatic vortex flowmeter, Flow Meas. Instrum. 2 (3) (1991) 169–179.
[10] R.C. Mottram, Vortex flowmeters—installation effects, Flow Meas. Instrum. 2 (1) (1991) 56–60.
[11] A. Laneville, A. Strzelecki, P. Gajan, P. Hebrard, Signal quality of a vortex flowmeter exposed to swirling flows, Flow Meas. Instrum. 4 (3) (1993) 151–154.
[12] M. Takamoto, H. Utsumi, N. Watanabe, Y. Terao, Installation effects on vortex shedding flowmeters, Flow Meas. Instrum. 4 (4) (1993) 277–285.
[13] Y. Terao, M. Takamoto, Improvement of a vortex shedding flowmeter performance by placing a narrow gap around a bluff body base, Trans. Soc. Instr. Contr. Eng. Japan 35 (12) (1999) 1628–1630.
[14] M. Henry, Recent developments in self-validating (SEVA) sensors, Sensor Review, MCB University Press 21 (1) (2001) 16–22.
[15] B. Menz, Vortex flowmeter with enhanced accuracy and reliability by means of sensor fusion and self-validation, Measurement 22 (3-4) (1997) 123–128.
[16] R. Schäfer, M. Jungmann, R. Werthschütz, Self diagnosis in flow measurement by combining venturi- and vortex-principle, tm—Technisches Messen 67 (9) (2000) 361–366.
[17] J.E. Amadi-Echendy, H. Zhu, E.H. Higham, Analysis of signals from vortex flowmeters, Flow Meas. Instrum. 4 (4) (1993) 225–231.
[18] S. Perovic, E.H. Higham, P.J. Unsworth, Fault detection and flow regime identification based on analysis of signal noise from electromagnetic flowmeters, Proceedings of the Institution of Mechanical Engineers, Part E (special issue), J. Process Mech. Eng. 215 (2001) 283–294.
[19] F. Blischke, H. Meyr, Parametric frequency estimator for the analysis of vortex sensor signals, tm—Technisches Messen 56 (12) (1989) 470–476.
[20] C. Carlander, J. Delsing, Installation effects on an ultrasonic flow meter with implications for self diagnostics, Flow Meas. Instrum. 11 (2) (2000) 109–122.
[21] D.W. Clarke, T. Ghaoud, Validation of vortex flowmeters, Comp. Contr. Eng. J. 13 (5) (2002) 237–241.
[22] D.W. Clarke, T. Ghaoud, A dual phase-locked loop for vortex flow metering, Flow Meas. Instrum. 14 (2003) 1–11.
[23] W. Heisenberg, Die absoluten Dimensionen der Kármánschen Wirbelbewegung, Physik. Zeitschr. XXIII (1922) 363–366.
[24] C. Raman, M. Köhl, R. Onofrio, D.S. Durfee, C.E. Kuklewicz, Z. Hadzibabic, W. Ketterle, Evidence for a critical velocity in a Bose–Einstein condensed gas, Phys. Rev. Lett. 83 (13) (1999) 2502–2505.
[25] T. Winiecki, B. Jackson, J. McCann, C. Adams, Vortex shedding and drag in dilute Bose–Einstein condensates, J. Phys. B 33 (19) (2000) 4069–4078.
[26] K.R. Sreenivasan, P.J. Strykowski, D.J. Olinger, Hopf bifurcation, Landau equation, and vortex shedding behind circular cylinders, in: K.N. Ghia (Ed.), Proceedings of the Forum on Unsteady Flow Separation, 52, ASME, New York, 1986, pp. 1–13.
[27] M. Provansal, C. Mathis, L. Boyer, Benard–von Kármán instability: transient and forced regimes, J. Fluid Mech. 182 (1987) 1–22.
[28] M. Schumm, E. Berger, P.A. Monkewitz, Self-excited oscillations in the wake of two-dimensional bluff bodies and their control, J. Fluid Mech. 271 (1994) 17–53.
[29] P. Albarède, M. Provansal, Quasi-periodic cylinder wakes and the Ginzburg–Landau model, J. Fluid Mech. 291 (1995) 191–222.
[30] J. Dusek, P.L. Gal, P. Fraunié, A numerical and theoretical study of the first Hopf bifurcation in a cylinder wake, J. Fluid Mech. 264 (1994) 59–80.
[31] P.L. Gal, A. Nadim, M. Thompson, Hysteresis in the forced Stuart–Landau equation: application to vortex shedding from an oscillating cylinder, J. Fluids Struct. 15 (2001) 445–457.
[32] L. Arnold, Random Dynamical Systems, Springer, Berlin, 1998.
[33] J. Guckenheimer, P. Holmes, Nonlinear oscillations, dynamical systems and bifurcations of vector fields, in: Applied Mathematical Sciences, 42, Springer, New York, 1983.
[34] B. Boashash, Estimating and interpreting the instantaneous frequeny of a signal, Proc. IEEE 80 (4) (1992) 520–568.
[35] H. Risken, in: The Fokker–Planck Equation, 2, Springer, Berlin, 1989, pp. 374–413 Chapter 12.
[36] K. Seybold, H. Risken, On the theory of a detuned single mode laser near threshold, Z. Physik. 267 (1974) 323–330.